Spatially resolved l-CH3+ emission in the Horsehead PDR: on the need for a top-down hydrocarbon chemistry

Draft version February 10, 2015
Preprint typeset using LaTeX style emulateapj v. 5/2/11

SPATIALLY RESOLVED l-C_3H^+ EMISSION IN THE HORSEHEAD PHOTODISSOCIATION REGION: FURTHER EVIDENCE FOR A TOP-DOWN HYDROCARBON CHEMISTRY*

V.V. Guzmán[1], J. Pety[2,3], J.R. Goicoechea[5], M. Gerin[3,4], E. Roueff[6,4], P. Gratier[7,8], and K.I. Öberg[1]

Draft version February 10, 2015

ABSTRACT

Small hydrocarbons, such as C_2H, C_3H and C_3H_2 are more abundant in photo-dissociation regions (PDRs) than expected based on gas-phase chemical models. To explore the hydrocarbon chemistry further, we observed a key intermediate species, the hydrocarbon ion l-C_3H^+, in the Horsehead PDR with the Plateau de Bure Interferometer at high-angular resolution ($6''$). We compare with previous observations of C_2H and c-C_3H_2 at similar angular resolution and new gas-phase chemical model predictions to constrain the dominant formation mechanisms of small hydrocarbons in low-UV flux PDRs. We find that, at the peak of the HCO emission (PDR position), the measured l-C_3H^+, C_2H and c-C_3H_2 abundances are consistent with current gas-phase model predictions. However, in the first PDR layers, at the 7.7 μm PAH band emission peak, which are more exposed to the radiation field and where the density is lower, the C_2H and c-C_3H_2 abundances are underestimated by an order of magnitude. At this position, the l-C_3H^+ abundance is also underpredicted by the model but only by a factor of a few. In addition, contrary to the model predictions, l-C_3H^+ peaks further out in the PDR than the other hydrocarbons, C_2H and c-C_3H_2. This cannot be explained by an excitation effect. Current gas-phase photochemical models thus cannot explain the observed abundances of hydrocarbons, in particular in the first PDR layers. Our observations are consistent with a top-down hydrocarbon chemistry, in which large polyatomic molecules or small carbonaceous grains are photo-destroyed into smaller hydrocarbon molecules/precursors.

Subject headings: astrochemistry molecular data molecular processes ISM: abundances ISM: molecules photon-dominated region (PDR)

1. INTRODUCTION

Simple hydrocarbon molecules, such as C_2H, C_3H, C_3H_2 and C_4H are ubiquitous in the interstellar medium (ISM). They are easily observed in a large variety of sources, from diffuse (e.g. Lucas & Liszt 2000) to dark clouds (e.g. Wootten et al. 1980; Cox et al. 1989; Mangum & Wootten 1990). In Photon Dominated Regions (PDRs) they have been found to be almost as abundant as in dark, well-shielded clouds, despite the strong UV radiation compared to the mean interstellar radiation field (e.g., Fossé et al. 2000; Fuente et al. 2003; Teyssier et al. 2004; Pety et al. 2005). In contrast to high UV-flux PDRs ($\chi \sim 10^4 - 10^5$ relative to the Draine field; Draine 1978), like Mon R2 or the Orion Bar, where the observed hydrocarbon abundances can roughly be explained with pure gas-phase chemistry models (Cuadrado et al. 2014), in low-UV flux PDRs ($\chi \lesssim 100$) the current pure gas-phase chemical models fail to reproduce their high abundances. Teyssier et al. (2004) and Pety et al. (2005) proposed that another mechanism producing carbon chains must exist in addition to gas-phase chemistry. One such possibility, suggested by some laboratory experiments and theoretical calculations, is the fragmentation of polycyclic aromatic hydrocarbons (PAH) or very small carbonaceous grains (VSGs) due to the far-UV radiation field (Le Page et al. 2003; Montillaud et al. 2013, and references therein). Indeed, recent laboratory experiments have shown that the far-UV irradiation of interstellar hydrogenated amorphous carbon analogs leads to the efficient production of small hydrocarbons, such as CH_4 (Alata et al. 2014). The good spatial correlation between the mid-IR emission due to PAHs and the distribution of carbon chains found in the Horsehead nebula, a low-UV flux PDR ($\chi \sim 60$), provides some support for a hydrocarbon production mechanism starting from PAHs (Pety et al. 2005).

Using single-dish observations, Pety et al. (2012) reported the first detection of l-C_3H^+, a key intermediate species in the gas-phase formation of small hydrocarbons, toward the Horsehead PDR. l-C_3H^+ was later detected toward the Sgr B2(N) molecular cloud (McGuire et al. 2013). Brünken et al. (2014) measured the millimeter rotational spectrum of l-C_3H^+ in the laboratory and unambiguously confirmed the assignment of the observed lines in the Horsehead to the hydrocarbon ion, l-C_3H^+. Moreover, Botschwina et al. (2014) performed highly accurate quantum chemical calculations to study this ion

vguzman@cfa.harvard.edu

* Based on observations obtained with the IRAM Plateau de Bure interferometer and 30 m telescope. IRAM is supported by INSU/CNRS (France), MPG (Germany), and IGN (Spain).

[1] Harvard-Smithsonian Center for Astrophysics, 60 Garden Street, Cambridge, MA 02138, USA
[2] Institut de Radioastronomie Millimétrique (IRAM), 300 rue de la Piscine, 38406 Saint Martin d'Hères, France
[3] LERMA, Observatoire de Paris, École Normale Supérieure, PSL Research University, CNRS, UMR8112, F-75014, Paris, France
[4] Sorbonne Universités, UPMC Univ. Paris 06, UMR8112, LERMA, F-75005, Paris, France
[5] Instituto de Ciencia de Materiales de Madrid (CSIC). E-28049 Cantoblanco, Madrid, Spain
[6] LERMA, Observatoire de Paris, PSL Research University, CNRS, UMR8112, F-92190 Meudon, France
[7] Univ. Bordeaux, LAB, UMR 5804, F-33270, Floirac, France
[8] CNRS, LAB, UMR 5804, F-33270, Floirac, France

TABLE 1
Observation parameters for the maps. Their projection center is $\alpha_{2000} = 05^h40^m54.27^s$, $\delta_{2000} = -02°28'00''$.

Line	Frequency GHz	E_u/k K	Instrument	Beam arcsec	PA °	Vel. Resol. km s^{-1}	Int. Time[b] hours	T_{sys} K (T_A^*)	Noise K (T_{mb})
c-C_3H_2 $2_{2,1} - 1_{0,1}$	85.339	6.4	PdBI/C&D	6.1×4.7	36	0.2	12.0	–	0.30
C_2H $N = 1 - 0$[a]	87.317	4.2	PdBI/C&D	7.2×5.0	54	0.2	12.0	–	0.60
l-C_3H^+ $J = 5 - 4$	112.446	16.2	PdBI/C&D	6.2×5.5	25	0.2	17.3	150	0.07
DCO^+ $J = 2 - 1$	144.077	10.4	30m/CD150	18.0×18.0	0	0.1	1.5	230	0.10

[a] Transition: $N = 1 - 0, J = 3/2 - 1/2, F = 2 - 1$. [b] On-source integration time scaled to a 6 antenna array.

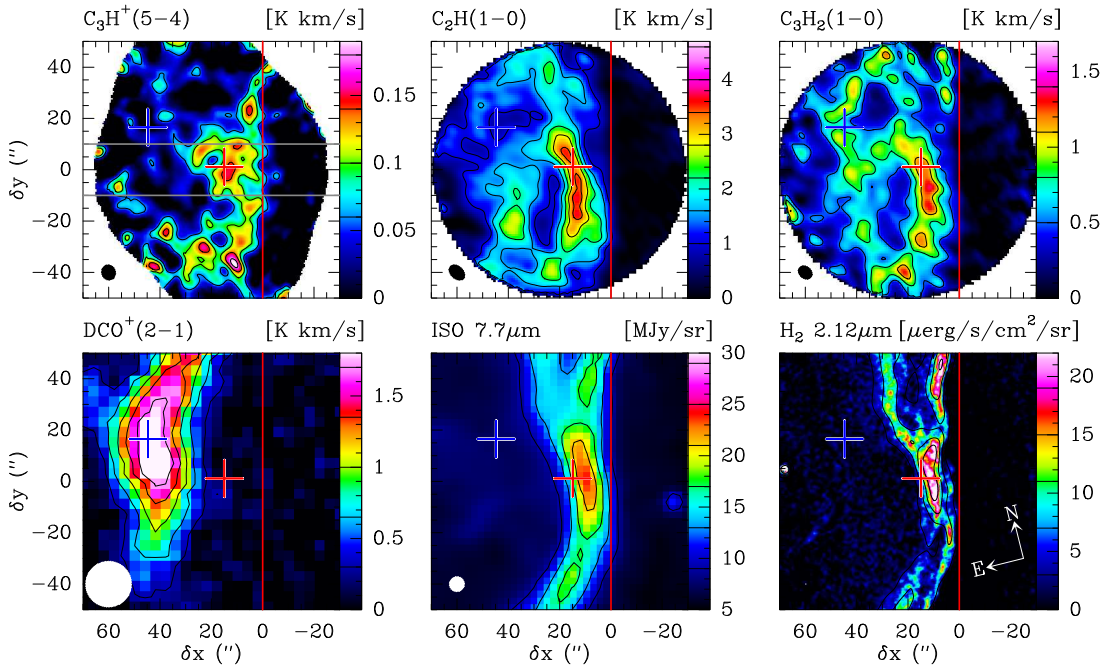

Fig. 1.— Integrated intensity maps of the small hydrocarbons l-C_3H^+, C_2H and c-C_3H_2 lines (upper row), as well as that of the DCO^+ line, the 7.7 μm PAH emission and the H_2 2.12 μm ro-vibrational line (bottom row). Maps have been rotated by 14° counter-clockwise around the projection center, located at $(\delta x, \delta y) = (20'', 0'')$, to bring the illuminating star direction in the horizontal direction and the horizontal zero has been set at the PDR edge, delineated by the red vertical line. The blue and red crosses show the Core and PDR positions, respectively. The two gray horizontal lines on top of the l-C_3H^+ map display the region over which the spectra are averaged in Fig. 2. All maps have been integrated between 10.1 and 11.1 km s^{-1}.

and found an excellent agreement with the spectroscopic constants derived from the observations in the Horsehead. More recently, Cuadrado et al. (2014) detected the l-C_3H^+ lines up to $J = 13$ in the Orion Bar, what allowed them to further refine the rotational constants. In addition, Mladenović (2014) revised the spectroscopic parameters of l-C_3H^+ by means of numerically exact rovibrational calculations. The detection of the small hydrocarbon l-C_3H^+ has thus been confirmed, both theoretically and experimentally.

Chemically, C_3H^+ is a gas-phase precursor of the small hydrocarbons C_3H and C_3H_2. Observations of the distribution of C_3H^+ with respect to these hydrocarbons could thus be used to constrain the dominant formation mechanism of small hydrocarbons. The Horsehead Nebula provides an ideal test-bed because it is viewed almost edge-on, providing easy access to the warm surface layer of a cloud where C^+ and therefore C_3H^+ is predicted to be the most abundant. As this warm photo-active layer is spatially narrow ($\sim 5''$, Guzmán et al. 2012), high angular resolution is needed to resolve the steep gradients in this region. To explore the relationship of C_3H^+ with its environment and with neutral carbon chains, we present in this letter the first spatially resolved observations of l-C_3H^+.

2. OBSERVATIONS

We used the Plateau de Bure Interferometer (PdBI) to obtain a 6″ angular resolution map of the emission of the l-$C_3H^+(5-4)$ line at 112.446 GHz. The observation parameters are summarized in Table 1. The observations were carried out in December 2012, April, May, September and October 2013 with six antennas in the C and D configurations (baseline lengths between 24 and 176 m). We observed a 9-field mosaic and used about 37 hours of telescope time, which correspond to 17.3 hours of on-source time scaled to a six antenna array after filtering out low-quality visibilities. The l-C_3H^+ line was covered with a correlator window of 20 MHz bandwidth and 39 kHz channel spacing. The typical precipitable water vapor amounted to 6 mm and the typical system temperature was 150 K.

The PdBI data was calibrated with the GILDAS[10]/CLIC software. The bright quasars 3C84, 2200+420 and 3C279 were used to calibrate the radio-frequency bandpass, and two nearby quasars (0420−014 and 0528+134) were regularly observed to calibrate phase and amplitude temporal variations. MWC349 was used to derive the absolute flux scale. In order to recover the extended emission that is filtered out by the PdBI, we observed the same region with the IRAM-30m telescope during ~ 15 hours of average summer weather in July and October 2013. The GILDAS/CLASS software was used to process the IRAM-30m data and produce the single-dish map, which was then combined with the PdBI observations in GILDAS/MAPPING, in the same way as described in Guzmán et al. (2013).

3. RESULTS

3.1. *Spatial distribution*

Fig. 1 displays the integrated intensity maps, at similar angular resolution ($6''$), of the l-C_3H^+ $J = 5-4$, C_2H $N = 1-0, J = 3/2-1/2, F = 2-1$ and c-C_3H_2 $2_{2,1}-1_{0,1}$ lines (Pety et al. 2005). Also displayed are the 7.7 μm emission arising from PAHs imaged with ISO at $6''$ angular resolution (Abergel et al. 2003), and the integrated intensity maps of the DCO^+ $J = 2-1$ line observed with the IRAM-30m telescope (Pety et al. 2007) and the H_2 $v = 1-0$ $S(1)$ line obtained with SOFI/NTT at $1''$ angular resolution (Habart et al. 2005).

The emission of the C_2H and c-C_3H_2 lines is structured into two successive filaments parallel to the dissociation front. The first one mainly coincides with the PDR, where intense emission is seen both in the H_2 rovibrational line and in the PAH mid-infrared band. The second one is located at the position of the cold dense UV-shielded core as indicated by the bright DCO^+ emission, with a difference between the two species: At the peak of the DCO^+ emission there is a clear, localized deficit of the C_2H emission compared to that of c-C_3H_2. In contrast, the l-C_3H^+ $J = 5-4$ line only emits toward the UV-illuminated edge, at the surface of the cloud. Moreover, the l-C_3H^+ emission reaches the red line in Fig. 1, which traces the edge of the PDR, while the emission of the two other hydrocarbons is shifted left of this line. We note that the observed l-C_3H^+ line is weak (6σ at the PDR), and hence the clumpy structure is most likely an artifact caused by the low signal-to-noise ratio. Indeed, due to the low inclination of the source the dirty beam has side-lobes which produce some uncertainty in the deconvolution of the data.

Line spectra along the direction of the illuminating star, centered at $dy = 0''$, are shown in the upper panel of Fig. 2. To increase the signal-to-noise ratios we have averaged the spectra over $20''$ in the dy-direction, *i.e.*, the region between the two gray lines in Fig. 1. In the bottom panel the integrated line intensity profiles of the hydrocarbons are shown, as well as that of the H_2 line and the PAH emission. The dashed vertical lines mark three characteristic positions in the Horsehead: the Core, corresponding to the peak of the DCO^+ line emission (RA $= 5^h40^m55.61^s$, Dec $= -2°27'38''$, J2000), and characteristic of the cold UV-shielded gas (marked by the blue cross in Fig 1); the PDR, corresponding to the peak of the HCO line emission emission (RA $= 5^h40^m53.936^s$, Dec $= -2°28'00''$, J2000; Gerin et al. 2009) and characteristic of the warmer UV-illuminated gas (marked by the red cross in Fig. 1); and a position closer to the edge of the cloud, corresponding to the peak of the 7.7 μm PAH emission (RA $= 5^h40^m53.6^s$, Dec$= -2°28'1.9''$, J2000). We observe a shift between the peak of l-C_3H^+ emission compared to that of the other hydrocarbons. l-C_3H^+ peaks at $\delta x \sim 10''$, while the other hydrocarbons peak at $\delta x \sim 15''$. Although the peak position of the l-C_3H^+ line has a higher uncertainty given the lower signal-to-noise ratio, the emission profile is clearly broader and it extends further out in the PDR compared to the C_2H and c-C_3H. Moreover, the l-C_3H^+ integrated line intensity profile correlates better to that of the H_2 line and the PAHs emission compared to neutral hydrocarbons.

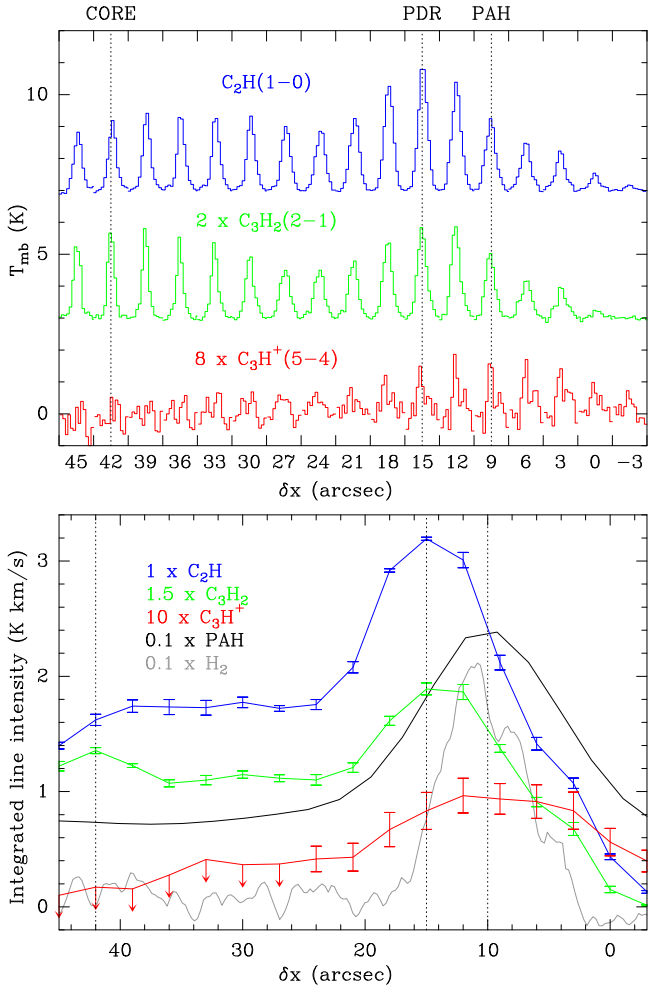

FIG. 2.— *Left:* Spectra along the direction of the exciting star at the PDR position ($dy = 0$ in Fig. 1), averaged over $20''$ in the dy-direction. *Right:* Integrated line intensities along the direction of the exciting star at the PDR position.

3.2. *Abundances*

To compare with chemical models, we have computed the column densities of C_2H, C_3H, C_3H_2 (both linear and cyclic species) and l-C_3H^+ at three different positions, namely the Core, PDR and PAH positions. These positions are slightly different from those used by Pety et al.

[10] See http://www.iram.fr/IRAMFR/GILDAS for more information about the GILDAS softwares (Pety 2005).

TABLE 2
Column densities and abundances with respect to H nuclei.

	CORE	PDR	PAH
$N_{\rm H}$	6.4×10^{22} cm^{-3}	3.8×10^{22} cm^{-3}	6.4×10^{21} cm^{-3}
$N(C_2H)$	$< 8.8\times10^{13}$	$(1.3-1.6)\times10^{14}$	$(1.5-5.0)\times10^{14}$
$N(c\text{-}C_3H)$	$(0.8-2.3)\times10^{12}$	$(2.4-7.2)\times10^{12}$	-
$N(l\text{-}C_3H)$	$(1.4-4.2)\times10^{11}$	$(0.6-1.8)\times10^{12}$	-
$N(o\text{-}c\text{-}C_3H_2)$	$(2.3-3.0)\times10^{12}$	$(3.8-6.9)\times10^{12}$	$(1.2-2.7)\times10^{13}$
$N(p\text{-}c\text{-}C_3H_2)$	$(0.6-1.1)\times10^{12}$	$(1.2-1.9)\times10^{12}$	-
$N(l\text{-}C_3H_2)$	$(0.9-2.6)\times10^{11}$	$(0.5-1.5)\times10^{12}$	-
$N(l\text{-}C_3H^+)$	$< 6.5\times10^{10}$	$(1.6-4.8)\times10^{11}$	$(1.4-4.1)\times10^{11}$
$X(C_2H)$	$< 1.8\times10^{-9}$	$(1.9-5.9)\times10^{-9}$	$(1.3-9.0)\times10^{-8}$
$X(C_3H)$	$(0.9-5.1)\times10^{-11}$	$(0.5-2.7)\times10^{-10}$	-
$X(C_3H_2)$	$(2.8-8.8)\times10^{-11}$	$(0.9-3.2)\times10^{-10}$	$(1.5-6.6)\times10^{-9}$
$X(l\text{-}C_3H^+)$	$< 1.7\times10^{-12}$	$(0.2-1.4)\times10^{-11}$	$(1.2-7.2)\times10^{-11}$

(2005) and Pety et al. (2012), and were chosen to take advantage of Horsehead WHISPER line survey. For the first two positions, we used the single-dish deep integrations obtained in the line survey and included beam dilution factors obtained from the higher-angular resolution PdBI observations when available. As no line survey has been made at the PAH position, we derived the abundances directly from the PdBI observations. For C_3H, we assumed the same spatial distribution of c-C_3H_2. We used the non-LTE radiative transfer code RADEX (van der Tak et al. 2007) for those species with known collisional rates, *i.e.*, C_2H and c-C_3H_2 (ortho and para), taken from Spielfiedel et al. (2012) and Chandra & Kegel (2000), respectively. The gas density was fixed to 6×10^4 cm^{-3} in the PDR, 10^5 cm^{-3} in the dense core (Gerin et al. 2009; Pety et al. 2007) and $(5-10)\times10^3$ cm^{-3} in the PAH position. The kinetic temperature was left as a free parameter, the best fits being consistent with previous estimates of ~ 60 K and ~ 20 K in the PDR and dense core, respectively. For C_3H and l-C_3H_2 we constructed rotational diagrams. We note that C_2H and l-C_3H^+ are not detected at the core position in the PdBI maps. We thus consider their derived abundances as upper limits. The inferred column densities and abundances with respect to total hydrogen nuclei are summarized in Table 2. The errors in the abundances take into account a 50% uncertainty in the assumed $N_{\rm H}$, which are inferred from the 1.2 mm dust continuum emission.

Pety et al. (2012) derived the l-C_3H^+ abundance at the PDR position using single-dish observations at $\sim 25''$ angular resolution, and computing a beam filling factors by assuming that the l-C_3H^+ emission filled a Gaussian filament of $\sim 12''$ width in the δx direction. This assumption was based on the morphology of the HCO line emission, which shows a filament of roughly this width. The new PdBI observations at $6''$ angular resolution show that the l-C_3H^+ emission indeed arises from a $\sim 12''$ filament, where the l-C_3H^+ $J=5-4$ line is ~ 3 times brighter than what was observed with the 30m.

3.3. *Chemistry*

In order to test our current knowledge of the gas-phase chemistry of hydrocarbons, we have used an updated version of the one-dimensional, steady-state photochemical code from Le Petit et al. (2006). The same model was used in Pety et al. (2012), except we have now introduced the formation and destruction (by H_2) rates of C_3H^+ measured by Savić & Gerlich (2005), which have an inverse temperature dependence. For the physical conditions in the Horsehead ($n_{\rm H}\simeq 6\times10^4$ cm^{-3}, $T_{\rm kin}\sim 60$ K), this results in higher abundances of C_3H and C_3H_2. The model includes grain surface reactions for the formation of H_2 and other species, such as H_2CO and CH_3OH, but only gas-phase reactions for the formation of hydrocarbons (see Pety et al. 2012, for a detailed description of the model).

In high UV-flux PDRs ($T_{\rm kin}\sim 100-500$ K), the formation of hydrocarbons starts with the formation of CH^+ (Cuadrado et al. 2014) through the very endothermic reaction $C^+ + H_2 \rightarrow CH^+ + H$ (Agúndez et al. 2010). In the Horsehead PDR, on the other hand, we find that the hydrocarbon gas-phase chemistry is initiated by reactions of C^+ with CH leading to C_2^+. Further reactions with H_2 lead to the formation of C_2H^+, $C_2H_2^+$ and $C_2H_3^+$. The last two species recombine with electrons to form C_2H and C_2H_2, respectively. C_2H_2 can react with C^+ to form C_3H^+, but in fact the dominant formation route of C_3H^+ at the edge of the cloud involves reactions between C_2H and C^+ leading to C_3^+, followed by reactions with H_2 in the model. Once C_3H^+ is produced, it reacts with H_2 to form the $C_3H_2^+$ and $C_3H_3^+$ ions which then recombine with electrons to form C_3H and C_3H_2. C_3H^+ can also recombine with electrons to form C_2H, although the dominant formation route for C_2H is the recombination of $C_2H_2^+$ with electrons:

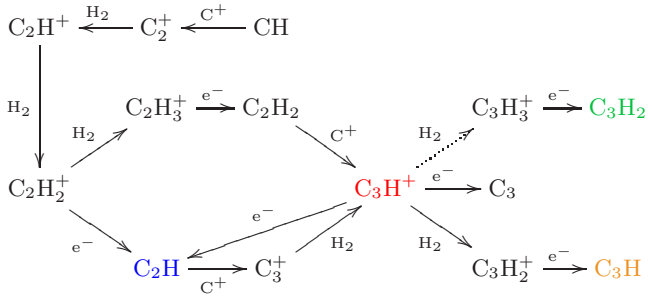

The dotted arrow in the scheme above marks a radiative association reaction, and the gray arrows indicate reactions with a temperature dependence of the rates. The C_3H^+ hydrocarbon ion is thus a key chemical pre-

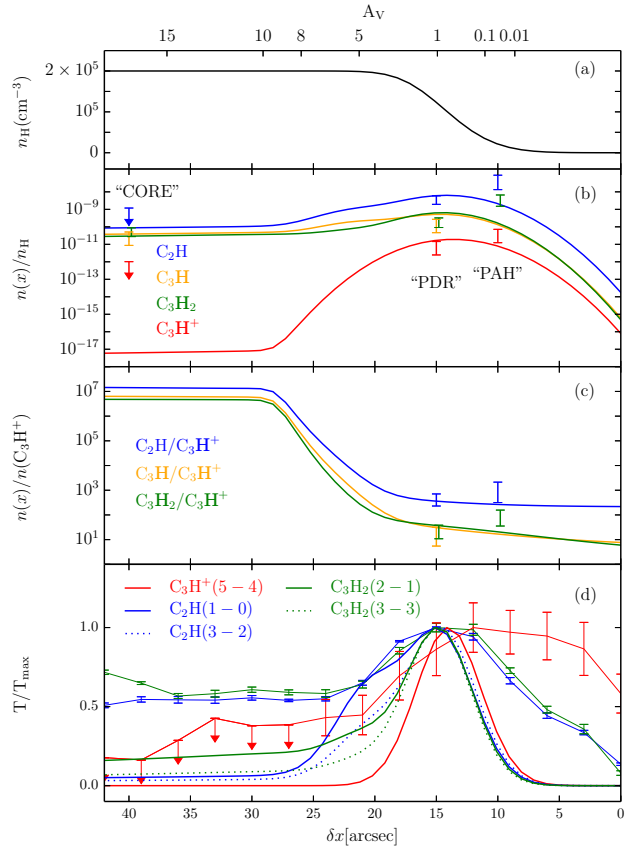

FIG. 3.— Photochemical model of the Horsehead PDR. (a) Density profile $n_H = n(H) + 2n(H_2)$. (b) Predicted abundance of small hydrocarbons. (c) Predicted abundance ratio relative to l-C_3H^+. (d) Predicted intensity profile. Two lines are included for C_2H: $N = 1 - 0$ ($E_u/k \sim 4$ K) and $N = 3 - 2$ ($E_u/k \sim 25$ K); and for c-C_3H_2: $J = 2 - 1$ ($E_u/k \sim 6$ K) and $J = 3 - 2$ ($E_u/k \sim 16$ K). The observed intensity profile is overlaid with error bars.

cursor of the small hydrocarbons in the gas phase. In particular, one would expect C_3H^+ and C_3H_2 to have a similar spatial distribution if gas-phase chemistry alone is responsible for the observed C_3H_2 abundance.

Fig. 3 displays the results of the photochemical model convolved to a resolution of 6″ to facilitate the comparison with observations. The steep density profile of the Horsehead is shown in the upper panel (a). The abundances with respect to total hydrogen nuclei are shown in panel (b). The abundance ratios with respect to l-C_3H^+ are shown in the panel (c). The observations are shown with error bars. In general, the abundances are well-reproduced by the pure gas-phase model at the PDR position ($A_V \simeq 1.5$). At the PAH position ($A_V \simeq 0.05$), on the other hand, the C_2H and c-C_3H_2 abundances are underpredicted by an order of magnitude. The same conclusion can be drawn from the abundance ratios, where the match between observations and model is better at the PDR than at the PAH position. We note that at the PAH position, the model better reproduces the observed l-C_3H^+ abundance than that of C_2H and C_3H_2. This suggests the need of an additional formation mechanism to explain the observed hydrocarbon abundances at the edge of the cloud.

The bottom panel (d) in Fig. 3 shows the modeled line intensity profile for each species and for different rotational transitions, normalized to their respective emission peaks. The observed profiles are overlaid with error bars. The modeled line intensity profiles of C_2H and c-C_3H_2 were computed by including the PDR model outputs (H_2 density, T_{kin} and column density) into the non-LTE radiative transfer code RADEX. In order to investigate excitation effects on the position of the emission peak, we included two transitions with different upper level energies for each species: the c-C_3H_2 $2_{1,2} - 1_{0,1}$ ($E_u = 6$ K) and C_2H $N = 1-0, J = 3/2-1/2, F = 2-1$ ($E_u = 4$ K) (solid lines), and the c-C_3H_2 $3_{1,2} - 3_{0,3}$ ($E_u = 16$ K) and C_2H $N = 3 - 2, J = 7/2 - 5/2, F = 3 - 2$ ($E_u = 25$ K) (dashed lines). These lines were chosen because their upper level energies are closer to that of the l-C_3H^+ $J = 5 - 4$ line ($E_u/k \sim 16$ K). Because there are no available collisional coefficients for l-C_3H^+, we assumed a constant excitation temperature along the cloud to compute its line intensity profile. In the model all hydrocarbons peak at the same position ($\delta x \sim 15''$). However, our observations show that the l-C_3H^+ emission peak is shifted compared to that of the other hydrocarbons. We note that the emission peak of C_2H and c-C_3H_2 does not change significantly between the lower and higher energy transitions. We have checked that including a constant excitation temperature for C_2H and c-C_3H gives similar results. This suggests that the excitation temperature gradient in the Horsehead takes place at very small spatial scales, and that the observed shift in the l-C_3H^+ emission peak compared to the other hydrocarbons is not due to an excitation effect but reveals a real difference in the spatial distribution of their column densities that is not predicted by the current pure gas-phase chemical models.

In general, the observed integrated intensity profile of all species is much broader than what the model predicts. In particular, the model underpredicts the l-C_3H^+ emission in the first PDR layers ($\delta x < 10''$). We run models with constant densities ($10^4 - 10^5$ cm^{-3}) to explore the effect of the density profile on the l-C_3H^+ intensity in the surface layers. We find that a higher density would slightly improve the agreement between model and observations, but it would not reproduce the observations of many other tracers (e.g., HCO, H_2, and dust continuum emission). Therefore, an additional formation mechanisms such as PAH photodestruction contributes to the formation of l-C_3H^+ in these surface layers. Indeed, it has been suggested that C_2H_2, which would enhance the C_3H^+ abundance through reactions with C^+, could be a product of photochemistry of PAHs (Bierbaum et al. 2011).

4. CONCLUSIONS

We have presented high-angular resolution (6″) observations of the hydrocarbon ion l-C_3H^+ in the Horsehead photo-dissociation region. The l-C_3H^+ emission is concentrated toward the surface edge of the nebula, close to where other hydrocarbon chains, such as C_2H and c-C_3H_2, and the 7.7 μm PAH emission peak. However, in contrast to C_2H and c-C_3H_2, l-C_3H^+ is only abundant in the first PDR layers with almost no emission deeper inside the cloud. l-C_3H^+ is thus a good tracer of hydrocarbon photo-chemistry. Moreover, l-C_3H^+ peaks $\sim 5''$ further outside the PDR than C_2H and c-C_3H_2, which cannot be explained by an excitation effect. This is in

contrast to what current gas-phase chemical models predict for the Horsehead physical conditions, that is, that all the hydrocarbons should peak approximately at the same position as their chemistry is closely linked.

The inferred l-C_3H^+ abundance at the PDR from the new high-resolution observations is consistent with that derived by Pety et al. (2012). In addition, we have computed the abundances of C_2H, C_3H_2 and l-C_3H^+ at three characteristic positions in the cloud. We find that a gas-phase chemical model can reproduce the hydrocarbon abundances, including the l-C_3H^+ abundance, at the PDR but it underpredicts the C_2H, c-C_3H_2 and l-C_3H^+ abundances at the PAH position, *i.e.*, at the edge of the cloud or the first PDR layers. The fact that the disagreement between model and observations occurs at the edge of the cloud, where the PAHs emission peaks, is consistent with a top-down hydrocarbon chemistry, where PAHs and small carbonaceus grains are photo-eroded by the radiation field releasing small hydrocarbons into the gas-phase. The Horsehead PDR is a clear case where this mechanism is efficient. Laboratory experiments are, however, needed to quantify the amount of hydrocarbons and the specific products that can be produced from this mechanism, and how this affects the hydrocarbon chemistry.

We thank the IRAM PdBI and 30 m staff for their support during the observations. This work was partially funded by the CNRS Programme Nationale de Physique et Chimie du Milieu Interstellaire (PCMI). J.R.G. thanks the Spanish MINECO for funding support from grants CSD2009-00038, AYA2009-07304 and AYA2012-32032. PG acknowledges funding from the ERC Starting Grant 3DICE (336474).

Facilities: IRAM:Interferometer, IRAM:30m.

REFERENCES

Abergel, A., Teyssier, D., Bernard, J. P., et al. 2003, A&A, 410, 577
Agúndez, M., Goicoechea, J. R., Cernicharo, J., Faure, A., & Roueff, E. 2010, ApJ, 713, 662
Alata, I., Cruz-Diaz, G. A., Muñoz Caro, G. M., & Dartois, E. 2014, A&A, 569, A119
Bierbaum, V. M., Le Page, V., & Snow, T. P. 2011, EAS Publications Series, 46, 427
Botschwina, P., Stein, C., Sebald, P., Schröder, B., & Oswald, R. 2014, ApJ, 787, 72
Brünken, S., Kluge, L., Stoffels, A., Asvany, O., & Schlemmer, S. 2014, ApJ, 783, L4
Chandra, S., & Kegel, W. H. 2000, A&AS, 142, 113
Cox, P., Walmsley, C. M., & Guesten, R. 1989, A&A, 209, 382
Cuadrado, S., Goicoechea, J. R., Pilleri, P., et al. 2014, arXiv:1412.0417
Draine, B. T. 1978, ApJS, 36, 595
Fossé, D., Cesarsky, D., Gerin, M., Lequeux, J., & Tiné, S. 2000, ISO Beyond the Peaks: The 2nd ISO Workshop on Analytical Spectroscopy, 456, 91
Fuente, A., Rodrıguez-Franco, A., Garcıa-Burillo, S., Martın-Pintado, J., & Black, J. H. 2003, A&A, 406, 899
Gerin, M., Goicoechea, J. R., Pety, J., & Hily-Blant, P. 2009, A&A, 494, 977
Guzmán, V. V., Goicoechea, J. R., Pety, J., et al. 2013, A&A, 560, A73
Guzmán, V., Pety, J., Gratier, P., et al. 2012, A&A, 543, LL1
Habart, E., Abergel, A., Walmsley, C. M., Teyssier, D., & Pety, J. 2005, A&A, 437, 177
Le Page, V., Snow, T. P., & Bierbaum, V. M. 2003, ApJ, 584, 316
Le Petit, F., Nehmé, C., Le Bourlot, J., & Roueff, E. 2006, ApJS, 164, 506
Lucas, R., & Liszt, H. S. 2000, A&A, 358, 1069
Mangum, J. G., & Wootten, A. 1990, A&A, 239, 319
McGuire, B. A., Carroll, P. B., Loomis, R. A., et al. 2013, ApJ, 774, 56
Mladenovi, M. 2014, J. Chem. Phys. 141, 224304
Montillaud, J., Joblin, C., & Toublanc, D. 2013, A&A, 552, AA15
Penzias, A. A., & Burrus, C. A. 1973, ARA&A, 11, 51
Pety, J. 2005, SF2A-2005: Semaine de l'Astrophysique Francaise, 721
Pety, J., Teyssier, D., Fossé, D., et al. 2005, A&A, 435, 885
Pety, J., Goicoechea, J. R., Hily-Blant, P., Gerin, M., & Teyssier, D. 2007, A&A, 464, L41
Pety, J., Gratier, P., Guzmán, V., et al. 2012, A&A, 548, A68
Pety, J., & Rodríguez-Fernández, N. 2010, A&A, 517, A12
Rodríguez-Fernandez, N., Pety, J., & Gueth, F. 2008, Single-dish observation and processing to produce the short-spacing information for a millimeter interferometer, IRAM Memo 2008-2
Savić, I., & Gerlich, D. 2005, Physical Chemistry Chemical Physics (Incorporating Faraday Transactions), 7, 1026
Spielfiedel, A., Feautrier, N., Najar, F., et al. 2012, MNRAS, 421, 1891
Teyssier, D., Fossé, D., Gerin, M., et al. 2004, A&A, 417, 135
Turner, B. E., Herbst, E., & Terzieva, R. 2000, ApJS, 126, 427
van der Tak, F. F. S., Black, J. H., Schöier, F. L., Jansen, D. J., & van Dishoeck, E. F. 2007, A&A, 468, 627
Wootten, A., Bozyan, E. P., Garrett, D. B., Loren, R. B., & Snell, R. L. 1980, ApJ, 239, 844